Highlights:

1) Spatial change in slip sense occurred along the Longmen Shan thrust belt (LSTB)
2) Qingchuan fault (QF) is a strike-slip-dominated active fault within the LSTB
3) Drainages and terraces are systematically deflected and/or offset along the QF
4) S-C fabrics of cataclastic rocks indicate a right-lateral strike-slip sense of the QF
5) Slip sense change along LSTB is mainly caused by the orientation of fault geometry

Structural analysis of the right-lateral strike-slip Qingchuan fault, northeastern segment of the Longmen Shan thrust belt, central China

Aiming Lin[1]*, Gang Rao[1,#] and Bing Yan[1,2]

[1]Department of Geophysics, Graduate School of Science,

Kyoto University, Kyoto 606-8502, Japan

[2]Graduate School of Science and Technology, Shizuoka University,

Shizuoka 422-8529, Japan

#Current address: Department of Earth Sciences, Zhejiang University

Hangzhou 310027, China

***Corresponding author:**
Department of Geophysics
Graduate School of Science
Kyoto University
Kyoto 606-8502, Japan
Tel & Fax: 81-75-753-3941
E-mail: slin@kugi.kyoto-u.ac.jp (A. Lin)

ABSTRACT

The eastern margin of the Tibetan Plateau is marked by the Longmen Shan thrust belt (LSTB), which is dominated by thrust faults and thrust-related fold structures that is home to the 2008 M_w 7.9 thrusting-type Wenchuan earthquake. Although previous works demonstrated that the seismogenic fault for the earthquake changed coseismic slip sense from thrust-dominated slip in the central and southeastern segments of the LSTB to right-lateral strike-slip-dominated displacement along the Qingchuan fault (northeastern segment of the LSTB), the related structures and current activity of the Qingchuan fault remains unclear. Topographic analyses of 0.5-m-resolution WorldView imagery and Digital Elevation Model (DEM) data, field investigations and structural analysis of the fault zone reveal that: i) stream channels and late Pleistocene–Holocene terrace risers and alluvial fans are systematically offset dextrally along the Qingchuan fault; ii) foliations developed in the fault zone indicate a right-lateral strike-slip-dominated displacement; and iii) geological evidence and seismic data show that the Qingchuan fault is

currently active as the main seismogenic fault dominated by a right-lateral strike-slip with an average slip rate of ca. 3–5 mm/yr. Our results demonstrate that the spatial change in slip sense along the LSTB from thrust-dominated in the central and southwestern sectors to right-lateral strike-slip-dominated in the northeastern sector is mainly caused by a change in the orientation of fault geometry from NE-SW to ENE-WSW along the LSTB.

Keywords: Longmen Shan thrust belt, Qingchuan fault, 2008 Wenchuan earthquake, right-lateral strike-slip, slip sense, Tibetan Plateau

1. Introduction

The Longmen Shan thrust belt (LSTB) separates the Tibetan Plateau to the west from the Sichuan Basin to the east, and is dominated by thrust faults and folds, where the 2008 M_w 7.9 thrusting-type Wenchuan earthquake occurred (Fig. 1). Our previous studies revealed that the 2008 earthquake produced a 285–300-km-long surface rupture zone, including a ca. 60-km-long segment along the Qingchuan fault in the northeastern sector of the LSTB (Lin et al., 2009, 2010a–c, 2012; Lin and Ren, 2009; Jia et al., 2010; Lin, 2011). In the 5 years since the 2008 M_w 7.9 Wenchuan earthquake, the understanding of the coseismic ground deformation features along the major active faults of the central and southwestern sectors of the LSTB (Lin et al., 2009, 2010a–c, 2012; Shen et al., 2009; Xu et al., 2009; Furuya et al., 2010; Hashimoto et al., 2010; Jia et al., 2010; Li et al., 2010; Zhang et al., 2010; Lin, 2011; Wang et al., 2013a), and of Holocene activity and paleoseismicity in those sectors (e.g., Lin et al., 2010d; Ran et al., 2010; Wang et al., 2013b) has improved, however, only a few studies have examined the tectonic topography and structural features of the Qingchuan

fault, in the northeastern sector of the LSTB (e.g., Burchfiel et al., 2008; Fan et al., 2008; Lin et al., 2012). The nature of the Qingchuan fault, including the slip sense, slip rate, and structures of fault zone, therefore, remains unclear due to a lack of geologic data. This limitation hinders further assessment of the tectonic history and the relationship between the pre-existing active faults and seismogenic activity.

In this study, to understand the nature and the deformation structures of the seismogenic fault within the northeastern sector of the LTSB, we integrated geomorphologic, geological, and seismic data including drainage patterns, offset terrace risers, fault zone structures, and focal mechanisms of large earthquakes along the Qingcuan fault.. We focus on the slip sense and recent activity of the Qingchuan fault and discuss the tectonic implications for the zone at the eastern margin of the Tibetan Plateau. This kind of study would help to improve our knowledge of relation between seismogenic faults and pre-existing geologic structures.

2. Seismotectonic setting

The study region lies in the northeastern sector of the LSTB, which demarcates the boundary between the eastern margin of the Tibetan Plateau and the Sichuan Basin (Fig. 1). The NE–SW-trending LSTB is dominated by thrust faults and fold structures developed mainly within pre-Mesozoic basement along the Longmen Shan Mountains over a distance of ca. 500 km and in a zone 30–50 km wide (Fig. 2). The LSTB contains four major thrust faults: the Wenchuan-Maowen, Yingxiu-Beichuan, Guanxian-Anxian, and Qingchuan faults (Figs 1 and 2), all of which were ruptured by the 2008 M_w 7.9 Wenchuan earthquake (Lin et al., 2010a–d). Seismic and geologic data show that the ca. 285–300-km-long rupture zone of this earthquake occurred along the LSTB (Fig. 1) (e.g., Lin et al., 2009, 2010a–c, 2012; Furuya et al., 2010; Jia et al., 2010; Hashimoto et al., 2010). Structural analyses of fault rocks show that three of the ruptured faults in the central and southwestern segments of the LSTB have moved as thrusts (Lin et al., 2010c). Previous studies reveal that these three faults, have reactivated throughout the late Quaternary, with slip rates of 1.0–3.0 mm/yr

(e.g., Li et al., 2006, 2010; Lin et al., 2010d) and probably ~1-10 mm/yr or larger although poorly constrained (Densmore et al., 2007). However, with respect to the Qinchuan fault to the NE, the kinematic behavior is less certain due to a lack of collection of geologic and geomorphic evidence concerning recent seismogenic activity on the fault (Deng, 2004).

Historic records document that more than 20 large earthquakes of M≥6, including five M≥7, occurred before the 2008 Wenchuan earthquake around and within the LSTB, but not on the Qingchuan fault (Editorial Board, Annals of Sichuan Province, 1998; CENC, 2008). Field investigations and trench excavations reveal that a great earthquake of M~8 occurred in the late Tang-Song Dynasty (AD 800–1000) and ruptured a >200-km-long thrust fault within the central and southwestern segments of the LSTB, along which coseismic ruptures also developed during the 2008 Wenchuan earthquake (Lin et al., 2010d). However, evidence is lacking to show that these or other large historic earthquakes occurred on the Qingchuan fault in the northeastern sector of the LSTB.

3. Tectonic geomorphology

Topographically, the Longmen Shan range reaches up to 7556 m above sea level (Mt. Gongga) and topographic relief more than 5 km over distances of less than 50 km (Fig. 1), representing one of the steepest mountain fronts along any margin of the Tibetan Plateau. The Qingchuan fault is developed in the northeastern part of the Longmen Shan range (Fig. 1), mainly within NE–SW-trending linear valleys (Fig. 3), and consists of several parallel to sub-parallel branch faults that are arrayed in a zone of <2 km in width and more generally <1 km (Figs 3 and 4). The topographic expression of the fault is characterized by straight linear traces with triangular facets, saddles, shutter ridges, and systematically offset or deflected stream channels (Figs 3–5). The triangular facets, which are mostly isosceles-triangle shaped, tend to be developed along the boundaries between the offset ridges and lowlands where the branch stream channels are also dextrally offset (Fig. 4). The offset and/or deflection of ridge spurs and river channels occur mainly in the mountain areas

where ridges are present across the fault (Fig. 3). Systematic deflection and/or offset of stream channels are observed at the eastern end of Bailong Lake, where the seismic rupture of the 2008 Wenchuan earthquake terminated (Fig. 3a and b). In this area, offset river channels across the fault can be restored to match channels of similar size (Fig. 3b and c). The deflection and/or offset amount of the stream channels ranges from several hundreds meters to 1.6 km (Fig. 4), and the restored dextral offset for the greatest number of matched stream channels is determined to be about 700 m (Fig. 3c). Generally, the main drainage elements show a combination structure that lateral offset and deflection of both ridge spurs and stream channels developed together across the fault as observed in the area between R8 and R11 (Fig. 3b, c). Similar features have also been observed along the San Andreas fault (e.g., Wallace, 1975). Such features make it difficult to accurately measure the amount of offset of drainage elements along the Qingchuan fault, as will be considered in the Discussion.

Typical geomorphic features associated with the dextral offset of river channels and associated fluvial terrace risers and alluvial fans are observed in the

Hanjiang River area at the northeastern end area of the study region, where three levels of terrace risers (T1–T3) are well developed along the Hanjiang River (Fig. 5). The offset stream channels and T2 terrace riser developed across the fault can be restored laterally about 58 m to optimize their fit with channels of similar size in width and terrace risers of string shape being matched across the fault trace (Fig. 5b). Thus, the T2 terrace riser and branch stream channels (R12 and R13) across the fault are dextrally offset about 58 m since its formation. The terrace risers on the northern side of the fault were displaced eastward to the stream channel of the Hanjiang River, where the fault developed within the basement rock is exposed. Distinct striations including grooves developed on the fault plane show a slip vector plunging 15°W, indicating a horizontal /vertical slip ratio of ~4:1 in displacement (Fig. 6). Accordingly, the measured amount of right-lateral offset represents the minimum accumulated displacement of the T2 riser, because the western margin of the T2 riser that bounded the river channel could have been eroded by the eastward-flowing river (Fig. 5).

4. Structures of fault zone

We investigated four representative exposures of the Qingchuan fault including the use of trenches to examine secondary structures and kinematic data (see Figs. 3a and 5a for locations).

4.1. Location 1

Location 1 occurs along the northeastern segment of the 2008 Wenchuan coseismic surface rupture zone on the Qingchuan fault (Fig. 7; see Fig. 3a for location). Faults are exposed along a large exposure that is >100 m in length and 30 m in height, which cut sedimentary basement rocks and alluvial deposits composed of interbedded sand-soil and sand-pebble layers (Fig. 7a). The main fault planes are marked by a thin gouge zone (3-10 cm thick) in the sand-soil sediments, showing yellow-brown in color (Fig 7b). Downthrown of the hanging wall sediments and slickenside striations (Fig. 7a) developed on a main fault plane bounded by the fault gouge zone (Fig. 7b and c) show a slip vector plunging 30°S, indicating a horizontal /vertical slip ratio of ~3:2.

4.2. Location 2

Location 2 is exposed at a construction site, where the 2008 Wenchuan coseismic ruptures occurred in a narrow zone (about 3 m wide) within a fault shear zone composed of cataclastic rocks, and four distinct fault planes show evidence of coseismic slip (Fig. 8a-c; Lin et al., 2012). The cataclastic rocks mainly consist of a wide zone of non-foliated cataclasite (>20 m in width) and a narrow fault breccia zone of 5-10 cm developed in the Mesozoic sedimentary rocks along the main fault planes. The main fault planes are marked by layers of fault gouge that are 2–3 cm thick, strike N10°–60°E, dip to the southeast at 10°–70°, and show an en echelon geometry (Fig. 8a and c). Slickenside striations developed on the main co-seismic fault plane show a slip vector plunging ~35°N, indicating a horizontal/vertical slip ratio of ~4:3 (Fig. 8b and d). This oblique movement sense is also observed along the fault scarps at this site, where two small gullies oriented perpendicular to the fault scarps are offset dextrally by 35 cm and vertically by 30 cm (Lin et al., 2012). The overprinting of co-seismic

surface ruptures on older cataclastic rocks including cataclasite, fault breccia, and fault gouge (Lin et al., 2010c), indicates a history of major faulting events within the Qingchuan fault zone.

4.3. Location 3

Location 3 is located at a fault scarp developed on the T2 terrace riser with a dextral offset of about 58 m (Fig. 5). The fault zone developed in the pre-Mesozoic marble basement rock consists of a foliated cataclasite zone of >3 m width and a thin fault gouge zone (1-2 cm thick) (Fig. 9a). Slickenside striations developed on the main fault show a strike-slip sense with a minor thrust component (Fig. 9b). S-C fabrics observed in X-Z section [using the terminology of Lin (1999, 2008) in this study] cut perpendicularly to the main foliation of the cataclasite and parallel to surfaces containing the slickenside striations plunging 8°W, showing a horizontal /vertical slip ratio of ~7:1 in displacement (Fig. 9c and d), coincident with the offset of terrace riser and branch river channels at this site.

4.4. Location 4

Location 4 is a trench site on the T2 terrace riser (Fig. 5a). For observing the fault zone structures and determining the formation age of T2 terrace riser, we dug out two trenches across the fault scarp (Trenches 1 and 2, see Fig. 5 for locations).

At Trench 1, the fault zone is developed within the marble basement bounded and overlain by unconsolidated organic-rich soil and sand-pebble sediments. Network fractures within the faulted marble are filled with brown-gray to dark-brown unconsolidated organic-rich soil (Fig. 10). The soil is >1.5 m thick on the downthrown (NW) side and contains dark-brown and dark-gray peaty materials and exhibits a random structure without sedimentary layering, covering the soil-sand pebble sediments (Figs 10b, c, and 11a).

The injection veins commonly have a complex geometry and occur as intricate networks within the cataclasite and can be locally traced back to the source unconsolidated dark-brown and dark-gray peaty materials bounded by the

fault plane (Fig. 11a). The injection veins terminate sharply along the fractures, which are similar with that of injected fault gouge vein observed in the fault outcrop at Loc. 3 (Fig. 11). Injection veins of fault gouge have also been reported in the southwest segments of the LSTB, which are suggested to be formed by repeated paleoseismic faulting events (Lin et al., 2010c; Lin, 2011). Radiocarbon dating results for the soil-silt layer covering the alluvial soil-sand-pebble sediments exposed at the base of the wall show that they formed at ca. 11000–17,000 yr BP (C02, 06–C08 in Table 1 and Fig. 10c).

At Trench 2, the fault zone was exposed in the marble basement (Fig. 12). To observe the structure of the fault zone, the trench walls were smoothed. The exposed fault zone is about 1 m wide between the cataclasitic marble and unconsolidated organic-rich soil-sand deposits (Fig. 12a and b). The foliated cataclasite zone is characterized by S–C fabrics observed in X–Z section (the base exposure wall of the Trench 2) (Fig. 12c). The S–surfaces are defined aggregates of marble fragments that are generally asymmetric in shape, the C–Surfaces are generally defined by subsidiary faults and discontinuous

fractures, and the C'–surfaces are defined by shear bands with fine-grained materials which are oblique to the C-surface (Fig. 12c). The orientations of S-C fabrics indicate a right-lateral strike-slip movement sense, coincident with that indicated by the offset T2 terrace riser (Fig. 5b) and that observed at Loc. 3 (Fig. 9).

5. Discussion

5.1. Offset and/or deflection of river channels

One of the most convincing lines of evidence for strike-slip faults in mountainous regions is the systematic offset of stream channels along the fault trace (e.g., Maruyama and Lin, 2002). Previous studies have shown such channels deflected along faults within the LSTB (e.g., Densmore et al., 2007; Fan et al., 2008).

In the present study region, most of the deflected stream channels and offset ridge spurs show more complicated geomorphic configurations than those reported previously. These configurations, such as the combination structures of

lateral offset and deflection with both right-lateral and left-lateral deflection, make estimating the offset magnitude from deflected river channels difficult. One example is from the Jialing River (Fig. 2), a main branch of the Yangtze River, where the maximum amount of dextral offset of the Jialing River along the Qingchuan fault was estimated to be up to 17 km (Fan et al., 2008). However, our interpretations of the topographic features do not support this estimate. If the Jialing River was dextrally offset by 17 km, the Xihanshui and Bailong rivers (Fig. 2), tributaries of the Jialing River with a similar channel scale, would have also been dextrally offset by a similar dextral amount. However, the Xihanshui River crosses the Qingchuan fault without distinct deflection (Fig. 2). Furthermore, the Bailong River shows an apparent left-lateral deflection of about 17–20 km along the Qingchuan fault, contrary to the right-lateral deflection of the Jialing River (Fig. 2). Therefore, these geomorphic features show that the main branches of the Yangtze River are not systematically offset or deflected along the Qingchuan fault.

In contrast, our analysis of a set of topographic features indicates a

systematic deflection of the drainage system along the eastern end of the Qingchuan fault with 1.6 km m in a dextral sense (Fig. 4c). Accordingly, we infer that this offset is the maximum recognizable dextral displacement accumulated along the Qingchuan fault. The striations developed on the main fault planes observed at the outcrops near Locs 3 and 4 where the T2 terrace riser has been offset about 58 m in dextral along the Qingchuan fault show a slip vector plunging 8°–30°W (Figs 6 and 9), which indicates that the horizontal/vertical slip ratio is ~4:1–7:1 in displacement. In contrast, the slip vectors inferred from the striations measured at Locs 1 and 2 indicate a horizontal/vertical slip radio is ~4:3–3:2. Furthermore, S-C fabrics of the foliated cataclastic rocks developed within the fault zone also indicate a right-lateral strike-slip shear sense (Figs 9, 11 and 12), coincident with that indicated by the topographical features. Based on this maximum offset amount of the mountain ridges and river channels and the offset amount of and 58 m of the T2 terrace riser, and the slip sense indicated by the striations developed on the main fault planes and S-C fabrics, we conclude that the Qingchuan fault is a right-lateral

strike-slip active fault and the dextral offset has been accumulated on the fault since the formation of the T2 terrace in the late Quaternary.

5.2. Rate of strike-slip motion

Estimation of slip rates across strike-slip faults requires the matching of displaced geomorphic and/or geologic reference markers, such as fluvial terrace risers, alluvial fans, and stratigraphic sequences that are datable. In the present study region, the three levels of terrace risers (T1, T2, and T3) along the Hanjiang River can be used as reference markers to estimate the slip rate along the Qingchuan fault. The T2 terrace riser, as well as the branch river channels developed within the T2 terrace riser, dextrally offset by about 58 m (Fig. 5b). Thus, the 58 m dextral offset accumulated since the formation of the T2 terrace riser. The trench investigations show that the soil-sand deposits containing peaty materials and covering the alluvial sand-gravel (pebble) deposits of the T2 terrace risers and fans yield radiocarbon dating ages of ca.11000-17000 yr BP (Fig. 10c; Table 1). We interpret the age to mean that the T2 terrace riser formed

synchronously in or just before ca. 17000 yr BP. Considering the formation time of the peaty material and age error range, we infer that the T2 terrace riser formed in the period between ca.11000 to ca. 20000 yr BP. Therefore, the average strike-slip rate is estimated to be 3–5 mm/yr for the most recent movement on the Qingchuan fault at this location.

5.3. Spatial change in slip sense along the active faults of the LSTB

Our previous studies (Lin et al., 2009, 2010a–c, 2012**)** showed that the 2008 coseismic surface ruptures overprint pre-existing fault traces of the Qingchuan fault and that coseismic right-lateral strike-slip displacements have accumulated upon the Qingchuan fault. This dominance of right-lateral strike-slip motion along the Qingchuan fault contrasts to that observed in the central and southwestern sectors of the Wenchuan rupture zone where thrusting dominates (e.g., Lin et al., 2009; Xu et al., 2009; Jia et al., 2010; Li et al., 2010**)**. The spatial change in slip sense from thrust-dominated slip in the central and southwestern sectors of the LSTB to right-lateral strike-slip-dominated

displacement in the northeastern sector of the LSTB along the Qingchuan fault probably reflects a change in the orientation of fault geometry from NE–SW in the southwestern-central sectors to ENE-WSW in the northeastern sector along the LSTB (Figs 1 and 13). The change in the fault orientation has been observed along the 2008 Wenchuan coseismic surface rupture zone along which the fault orientation changed from a general trend of N10°–40°E in the southwestern-central sectors to N45°–70° in the northeastern sector (Lin et al., 2009, 2012). Thus, the change in fault orientation may cause a change in kinematic behavior including slipping sense during individual large earthquakes along a seismogenic fault zone.

Long-term Global Positioning System (GPS) data show that the Tibetan Plateau is currently moving eastward, perpendicular to the general trend of the central and southwestern sectors of the LSTB, resulting in a compressive stress that is leading to the formation of fold–thrust structures. However, the eastern margin of the Tibetan Plateau, adjacent to the northeastern sector of the LSTB, is moving northeastward (Fig. 13a) (Zhang et al., 2004; Gan et al., 2007). GPS data

acquired after the 2008 earthquake reveal that the direction of ground motion differs on each side of the Qingchuan fault, being anticlockwise on the northwestern side of the fault and clockwise on the southeastern side (Wang et al., 2011). Right-lateral strike-slip movement is observed along the northeastern sector of the Qingchuan fault (Shen et al., 2009) (Fig. 13b). Analyses of ALOS/PALSAR (Advanced Observation Satellite/Phased-array type L-band Synthetic Aperture Radar) data also reveal that a major right-lateral coseismic slip occurred in the northeastern sector of the LSTB during the 2008 earthquake (Hashimoto et al., 2010). These geodetic data indicate a right-lateral strike-slip-dominated displacement along the Qingchuan fault, which concurs with our field observations. Focal mechanisms of large aftershocks ($M_w \geq 5$) associated with the 2008 Wenchuan earthquake also show that the faults in the northeastern sector around the Qingchuan fault have a right-lateral strike-slip-dominated displacement sense, and the central and southwestern sectors of the LSTB are dominated by a thrust slip (Fig. 13b). Therefore, the various data indicate a transition from a thrust-dominated style of

accommodation in the central and southwestern sectors to a right-lateral strike-slip-dominated style of accommodation in the northeastern sector (Qingchuan fault) of the LSTB. This spatial transition can also be considered to reflect a change in the orientation of fault geometry from NE-SW in the southwestern sectors to ENE-WSW in the northeastern sector along the LSTB as documented above. The amount of right-lateral strike-slip movement (up to 58 m) that accumulated on the T2 terrace risers in past ~20 kyr and the large horizontal/vertical slip ratio of up to 7:1 in displacement along the Qingchuan fault, as documented above, also supports the idea that the fault has played a role in releasing seismic energy as a right-lateral strike-slip seismogenic fault at the northeastern margin of the Tibetan Plateau.

6. Conclusions

Based on the results of topographic analysis from high-resolution WorldView imagery, field investigations, and trench excavations, we conclude that: (i) the Qingchuan fault is an active fault dominated by a right-lateral

strike-slip in the late Quaternary, (ii) systematic right-lateral offsets of up to ca. 1.6 km have occurred in elements of the drainage system along the Qingchuan fault, (iii) the average rate of right-lateral strike-slip motion in the late Pleistocene-Holocene is estimated to be ca. 3–5 mm/yr, with an average value of 4 mm/yr. Our results demonstrate that the spatial change in slip sense from thrusting-dominated slip in the southeastern sector to right-lateral-dominated slip in the northeastern sector of the LSTB along the Qingchuan fault is mainly caused by a change in the orientation of fault geometry from NE-SW to ENE-WSW along the LSTB.

Acknowledgements

We are grateful to Dr. M. Ellis and an anonymous reviewer and editor Prof. W.M. Dunne for their critical reviews that helped to improve the manuscript. We thank Dr. J. Hu, J. Fu, J. Du, H. Chen, and W. Gong for their assistance and discussion in the field. This work was supported by a Grant-in-Aid for Scientific Research (A) (No. 23253002 awarded to A. Lin) from the Ministry of Education,

Culture, Sports, Science, and Technology of Japan.

References

Burchfiel, B.C., Royden, L.H., van der Hilst, R.D., Hager, B.H., 2008. A geological and geophysical context for the Wenchuan earthquake of 12 May 2008, Sichuan, People's Republic of China. GSA Today 18, doi:10.1130/GSATG18A.J.

Bureau of Geology and Mineral Resource of Sichuan Province (BGMRSP), 1991. Regional Geology of Sichuan Province (Beijing: Geological Publishing House).

China Earthquake Networks Center (CENC), 2008. Rupture process of the 2008 Ms 8.0 Wenchuan Earthquake. http://www.cenc.ac.cn/ (last accessed, 10 Nov. 2013).

Deng, Q. (ed), 2004. Maps of active tectonics in China. 1:4,000,000, Seismological Press, Beijing.

Densmore, A.L., Ellis, M.A., Li, Y., Zhou, R., Hancock, G.S., Richardson, N.,

2007. Active tectonics of the Beichuan and Pengguan faults at the eastern margin of the Tibetan Plateau. Tectonics 26, TC4005, doi:10.1029/2006TC001987.

Editorial Board, Annals of Sichuan Province, 1998. Annals of Sichuan Province: Annals of Earthquake. Sichuan People Press, Chengdu, 382p.

Fan, C., Wang, E., Wang, G., Wang, S., 2008. Dextral strike-slip and tectonic transformation of the northern Longmen Shan fault belt from Late Neogene: A case study from the Qingchuan fault. Chinese Journal of Geology 43, 471–433.

Furuya, M., Kobayashi, T., Takada, Y., Murakami, M., 2010. Fault source modeling of the 2008 Wenchuan earthquake based on ALOS/PALSAR data. Bulletin of Seismological Society of America 100, 2750–2766.

Gan, W., Zhang, P., Shen, Z., Niu, Z., Wang, M., Wan, Y., Zhou, D., Cheng, J., 2007. Present-day crustal motion within the Tibetan Plateau inferred from GPS measurements. Journal of Geophysical Research 112, B08416, doi:10.1029/2005JB004120.

Harvard University, 2008. Global CMT Catalog, 200805120628A Eastern Sichuan, China (http://www.globalcmt.org/CMTsearch.html) (last accessed, 31 March 2014).

Hashimoto, M., Enomoto, M., Fukushima, Y., 2010. Coseismic deformation from the 2008 Wenchuan, China, earthquake derived from ALOS/PALSAR images. Tectonophysics 491, 59–71.

Jia, D., Li, Y., Lin, A., Wang, M., Chen, W., Wu, X., Ren, Z., Zhao, Y., Luo, L., 2010. Structural model of 2008 Mw 7.9 Wenchuan earthquake in the rejuvenated Longmen Shan thrust belt, China. Tectonophysics 491, 174–184.

Li, Y., Zhou, R., Densmore, A. L., Ellis. M.A., *et al.*, 2006. Continental dynamics and Geological responses of the eastern margin of Qinghai-Tibet Plateau. Geological Press, Beijing, 148p (in Chinese with English abstract).

Li, Y., Jia, D., Shaw, J., Hubbard, J., Lin, A., Wang, M., Luo, L., Li, H., Wu, L., 2010. Structural interpretation of the co-seismic faults of the Wenchuan earthquake: 3D modeling of the Longmen Shan fold-and-thrust belt. Journal of Geophysical Research 115, B04314, doi:1029/2009B006824

Lin, A., 1999. S-C cataclasite in granitic rock. Tectonophysics 304, 257–273.

Lin, A., 2008. Fossil Earthquakes: The Formation and Preservation of Pseudotachylytes. Springer, 348 pp.

Lin, A., 2011. Seismic slip recorded in the fluidized ultractaclastic veins formed along the coseismic shear zone during the 2008 M_w7.9 Wenchuan earthquake. Geology 39, 547–550.

Lin, A., Ren, Z., 2009. The Great Wenchuan Earthquake of 2008—A Photographic Atlas of Surface Rupture and Related Disaster. Springer, Berlin, 121p (ISBN:978-3-642-03758-0).

Lin, A., Ren, Z., Jia, D., Wu, X., 2009. Co-seismic thrusting rupture and slip distribution produced by the 2008 M_w7.9 Wenchuan earthquake, China. Tectonophysics 471, 203–215.

Lin, A., Ren, Z., Jia, D., 2010a. Co-seismic ground-shortening structures produced by the 2008 M_w7.9 Wenchuan earthquake, China. Tectonophysics 491, 21–34.

Lin, A., Ren, Z., Rao, G., 2010b. Eyewitness accounts of surface thrusting and

folding during the 2008 M_w7.9 Wenchuan earthquake, China. Seismological Research Letters 81, 884–891.

Lin, A., Ren, Z., Kumahara, Y., 2010c. Structural analysis of the coseismic shear zone of the 2008 M_w7.9 Wenchuan earthquake, China. Journal of Structural Geology 32, 781–791.

Lin, A., Ren, Z., Jia, D., Miyairi, Y., 2010d. Evidence for a Tang-Song great earthquake along the Longmen Shan Thrust Belt prior to the 2008 M_w7.9 Wenchuan earthquake, China. Journal of Seismology 14, 615–628.

Lin, A., Rao, G., Yan, B., 2012. Field evidence of rupture of the Qingchuan Fault during the 2008 M_w7.9 Wenchuan earthquake, northeastern segment of the Longmen Shan Thrust Belt, China. Tectonophysics 522-523, 243–252.

Maruyama, T., Lin, A., 2002. Active strike-slip faulting history inferred from offsets of topographic features and basement rocks: a case study of the Arima-Takatsuki Tectonic Line, southwest Japan. Tectonophysics 344, 81–101.

Ran, Y., Chen, L., Chen, J., Wang, H., Chen, G., Yin, L., Shi, X., Li, C., Xu, X.,

2010. Paleoseismic evidence and repeat time of large earthquakes at three sites along the Longmenshan fault zone. Tectonophysics 491, 141–153.

Shen Z., Sun, j., Zhang, P., Wan, Y., Wang, M., Burgmann, R., Zeng, Y., Gan, W., Liao, H., Wang Q., 2009. Slip maxima at fault junctions and rupturing of barriers during the 2008 Wenchuan earthquake. Nature Geoscience 2, 718–724.

Stuiver, M., Reimer, P. J., Reimer, R., 2003. CALIB Radiocarbon Calibration Version 4.4. http://radiocarbon. pa.qub.ac.uk/calib/. Last accessed, 10 Nov 2012).

Tian Y., Ning, J., Yu, C., 2013. Focal mechanism solution of the Wenchuan earthquake sequence from polarities and SH/P amplitude ratios: new results and implications. Earthquake Science, 26, 357-372.

United States Geological Survey, 2008. Magnitude 7.9 Eastern Sichuan, China (http://earthquake.usgs.gov/eqcenter/eqinthenews/2008/us2008ryan/) (last accessed, 10 Nov. 2012).

Wallace, R., 1975. The San Andreas fault in the Carrize plain-Tremblor Range

region, CA. Calif. Div. Mines and Geology Special Report, 118, 241-50.

Wang, Q., Qiao, X., Lan, Q., Freymueller, J., Yang, S., Xu, C., Yang, Y., You, X., Tan, K., Chen, G., 2011. Rupture of deep faults in the 2008 Wenchuan earthquake and uplift of the Longmen Shan. Nature Geoscience 4, 634–640.

Wang, M., Jia, D., Lin, A., Li, S., Rao, G., Li, Y., 2013a. Late Holocene activity and historical earthquakes of the Qiongxi thrust fault system in the southern Longmen Shan fold-and thrust belt, eastern Tibetan Plateau. Tectonophysics, 584, 102–113.

Wang, M., Jia, D., Shaw, J., Hubbard, J., Lin, A., Li, Y., Li, S., 2013b. Active Fault-Related Folding beneath an Alluvial Terrace in the Southern Longmen Shan Range Front, Sichuan Basin, China: Implications for Seismic Hazard. Bulletin of Seismological Society of America 103, 2369–2385.

Xu, X., Wen, X., Yu, G., Chen, G., Klinger, Y., Hubbard, J., Shaw, J., 2009. Coseismic reverse- and oblique-slip surface faulting generated by the 2008 M_w7.9 Wenchuan earthquake, China. Geology 37, 515–518.

Zhang, P., Shen, Z., Wang, M., Gan, W., Burgmann, R., Molnar, P., Wang, Q.,

Niu, Z., Sun, J., Wu, J., Sun, H., You. X., 2004. Continuous deformation of the Tibetan Plateau from global positioning system data. Geology 32, 9809–9812.

Zhang, P., Wen, X., Shen, Z., Chen, J., 2010. Oblique, high-angle, listric-reverse faulting and associated development of train: the Wenchuan earthquake of May 12, 2008, Sichuan, China. Annu. Rev. Earth Planet. Sci. 38, 353–382.

Figure Captions

Figure 1. Location maps showing topography of the Longmen Shan region and the distribution of coseismic surface ruptures of the 2008 Wenchuan earthquake [modified from Lin et al. (2009, 2010a)]. (a) Landsat image of the Tibetan Plateau and north India, showing the location of the study area. Yellow and red arrows indicate the direction of movement of the Tibetan Plateau and the Indian Plate, respectively. (b) SRTM (Shuttle Radar Topography Mission; 90 m resolution) color shaded-relief map showing the tectonic landforms of the Longmen Shan region. Red stars indicate epicenters of the 2008 Wenchuan earthquake [(CENC, 2008), Harvard University (Harvard, 2008), and the United States Geological Survey (USGS, 2008)].

Figure 2. Geological map of the study region, showing the geologic structures of the Longmen Shan region [modified from BGMRSP (1991) and Lin et al. (2012)]. The distribution of coseismic surface ruptures is modified from Lin et al. (2009).

Figure 3. Shuttle Radar Topography Mission (SRTM) color shaded-relief map (a) and remote-sensed image (from Google) (b, c) showing the tectonic landforms of the study region along the Qingchuan fault. (a) Coseismic surface ruptures by the 2008 Wenchuan earthquake along the Qingchuan fault, which (see Fig. 1b for location). (b) Drainage channels dextrally deflected and/or offset along the Qingchuan fault on the western side of Bailong Lake. R1– R1' to R8–R8' are river channels that are dextrally offset along the fault trace. (c) Restored map of the topography along the Qingchuan fault by about 700 m displacement.

Figure 4. Stereo maps compiled 0.5-m-resolution WorldView images and DEM data (30 m resolution) showing systematically-offset stream channels and terminal facets along the Qingchuan fault at eastern site of the study region (see Fig. 3a for location). The stream channels are dextrally offset by 0.9–1.6 km. The images in (a)–(c) form a continuous scene from east to west.

Figure 5. (a) Stereo map compiled 0.5-m-resolution WorldView images and DEM data (30 m resolution) (location shown in Fig. 4a); (b) restored map with location in Fig. 5a showing systematically-offset stream channels and alluvial terrace risers and fans in the Hanjiang River region. H: T2 and T3 terrace heights above current river channel in meters.

Fig. 6. (a) Topographic features of the offset T2 terrace riser in the area around Location 3 (see Fig. 5a for location). (b) Fault plane where striations (white arrows) are present. (c) Topographic features of the offset T2 terrace riser in the western site of Location 3 (see Fig. 5a for location). T2a and T2b indicate the dextrally-offset edge of T2 terrace riser. (d) Lower hemisphere equal-area stereographic projection showing the orientations of striations on the fault surface in (b), indicating a strike-slip-dominated slip sense. Long arrow indicates the slip vector of hanging wall. Contour interval is 5% per 1% area.

Figure 7. Photographs of representative fault outcrop at Location 1 (a, b) and

stereo projection of striations developed on the fault plane (c) (see Fig. 3a for location). (a) Overview of the outcrop exposure. Cataclasite-bearing basement rocks in the hanging wall of F1 fault are downthrown 20-30 m. White broken line indicates the top of basement rock in the hanging wall of F1 fault. Two mans marked by white ellipses show the scale. (b) Close-up view of secondary fault zone (F3) with 5–10 cm gouge zone (see Fig. 7a for location). The twisted sickle shown for scale is 25 cm in length. (c) Lower hemisphere equal-area stereographic projection for striations collected from the fault surface in Fig. 7b. Long arrow indicates the slip vector of hanging wall. Contour interval is 5% per 1% area.

Figure 8. (a) General view of Location 2 (see Fig. 3a for location). Note that the coseismic surface ruptures (indicated by red arrows) transect the cataclasite-bearing host rock. (b) Close-up view of a fault zone containing fault gouge zone where the striations are observed. (c) Close-up view showing ruptures transecting cataclasite. (d) Lower hemisphere equal-area stereo

projection of striations showing the orientations of striations on coseismic fault surface in (b). Long arrow indicates the slip vector of hanging wall. Contour interval is 5% per 1% area.

Figure 9. (a) Overview of Location 3 (see Fig. 5a for location). The hammer shown for scale is 35 cm in length. (b) Lower hemisphere equal-area stereographic projection showing the orientations of striations on the coseismic fault plane shown in (a). Long arrow indicates the slip vector of hanging wall. Contour interval is 5% per 1% area. (c) Close-up view of the fault exposed in (a). The pen shown for scale is 14 cm in length. (d) Polished section of hand specimen from (c). Note that S-C fabrics show a dextral slip sense.

Figure 10. P Trench 1 at Location 4 (see Fig. 5a for location). (a) Overview of trench. The tape measure shown for scale is 2 m in length. (b) West exposure wall. Grid interval is 1 m. (c) Sketch of (b). Note network soil veins injected into the fault-fracture zone of the marble footwall rock. ^{14}C dating ages are shown in

Table 1.

Figure 11. (a) Injection soil veins exposed in Trench 1 at Location 3. Grid interval is 1 m. (b) Injection gouge vein exposed at Location 4. The twisted sickle shown for scale is 25 cm in length. Note that both the injection veins of soil and fault gouge can be traced back to the source materials bounded by the fault plane.

Figure 12. Photographs of the wall exposed in Trench 2 at Location 4. (a) Fault boundary between the marble basement and surface soil-clay deposits observed on the southwest wall. Grid interval is 1 m. (b) Foliated cataclasite zone observed in the marble basement rock of northeast wall. (c) Close-up view of fault zone observed at the base exposure of the trench shown in (a).

Figure 13. Surface displacement inferred from GPS measurements of the eastern margin of the eastern Tibetan plate around the LSTB. (a) Displacement vectors

with respect to the Eurasia fixed reference frame indicate the direction of movement of the Tibetan Plateau and of the LSTB before the 2008 Wenchuan earthquake [GPS data are from Zhang et al. (2004) and Gan et al. (2007)]. (b) Coseismic slip distribution and movement sense of the ground surface around the LSTB caused by the 2008 Wenchuan earthquake [GPS data are from Wang et al. (2011), focal mechanism data from Tian et al., (2013)].

Figure1

Click here to download high resolution image

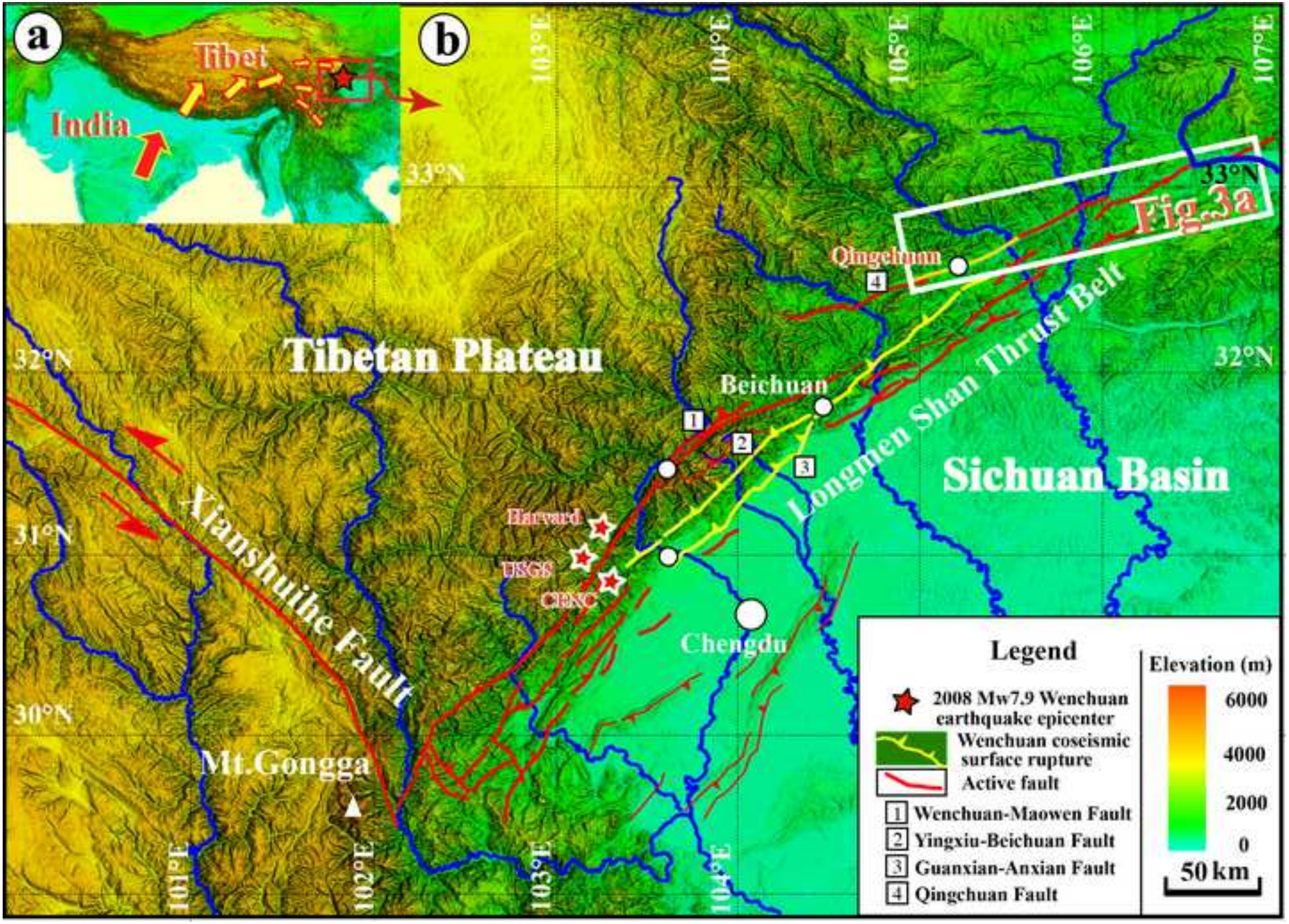

Figure2

Click here to download high resolution image

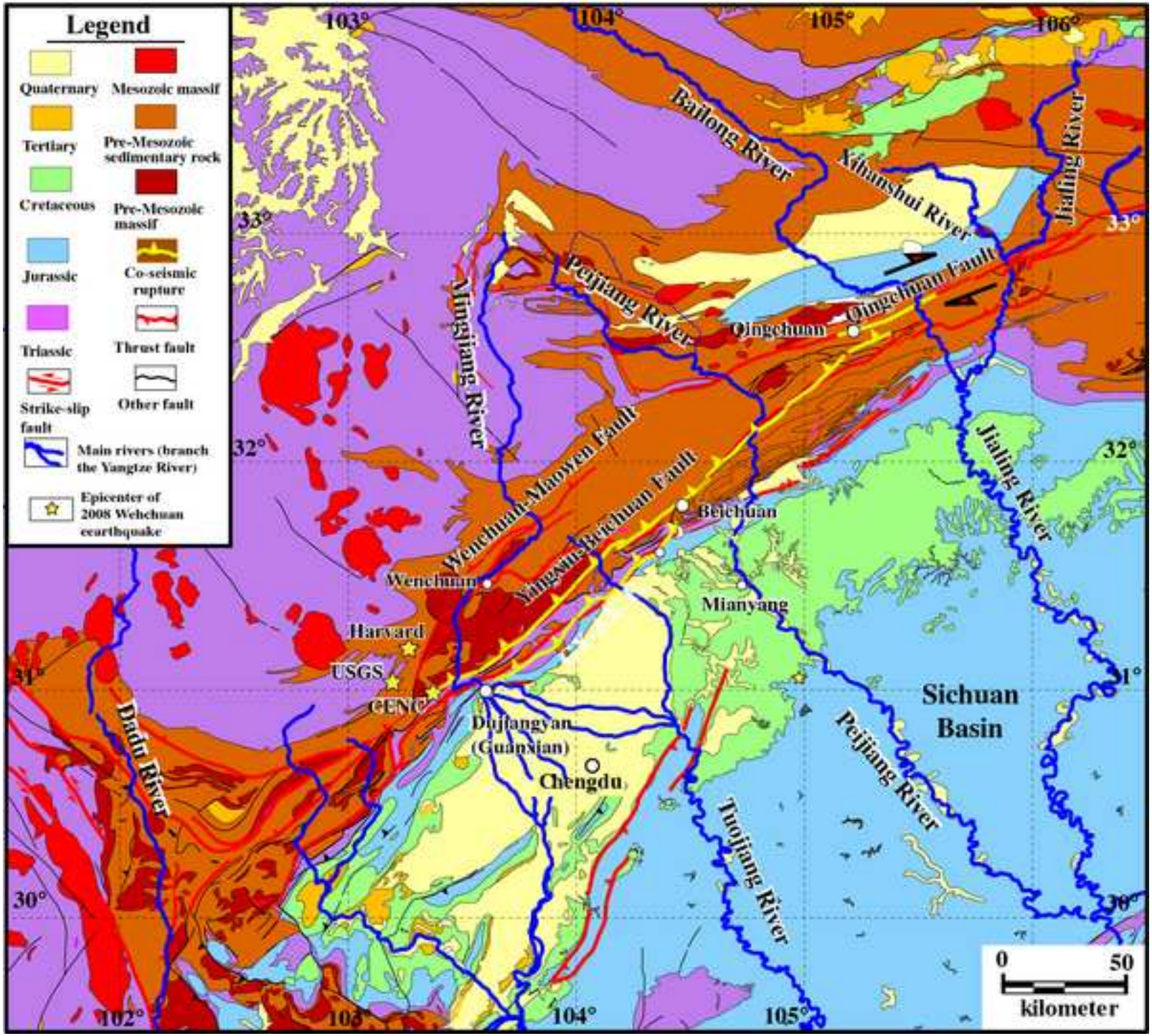

Figure3

Click here to download high resolution image

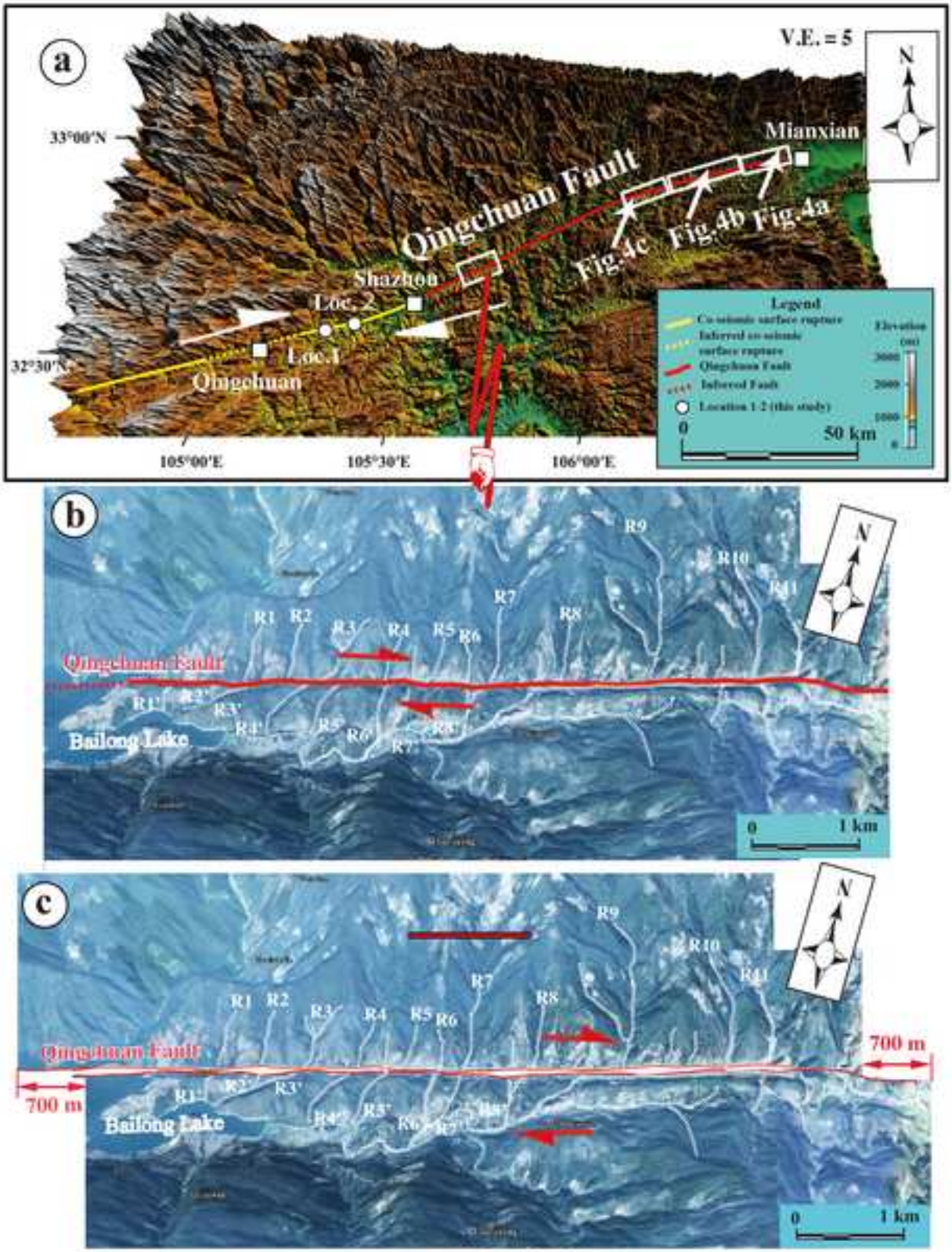

Figure4

Click here to download high resolution image

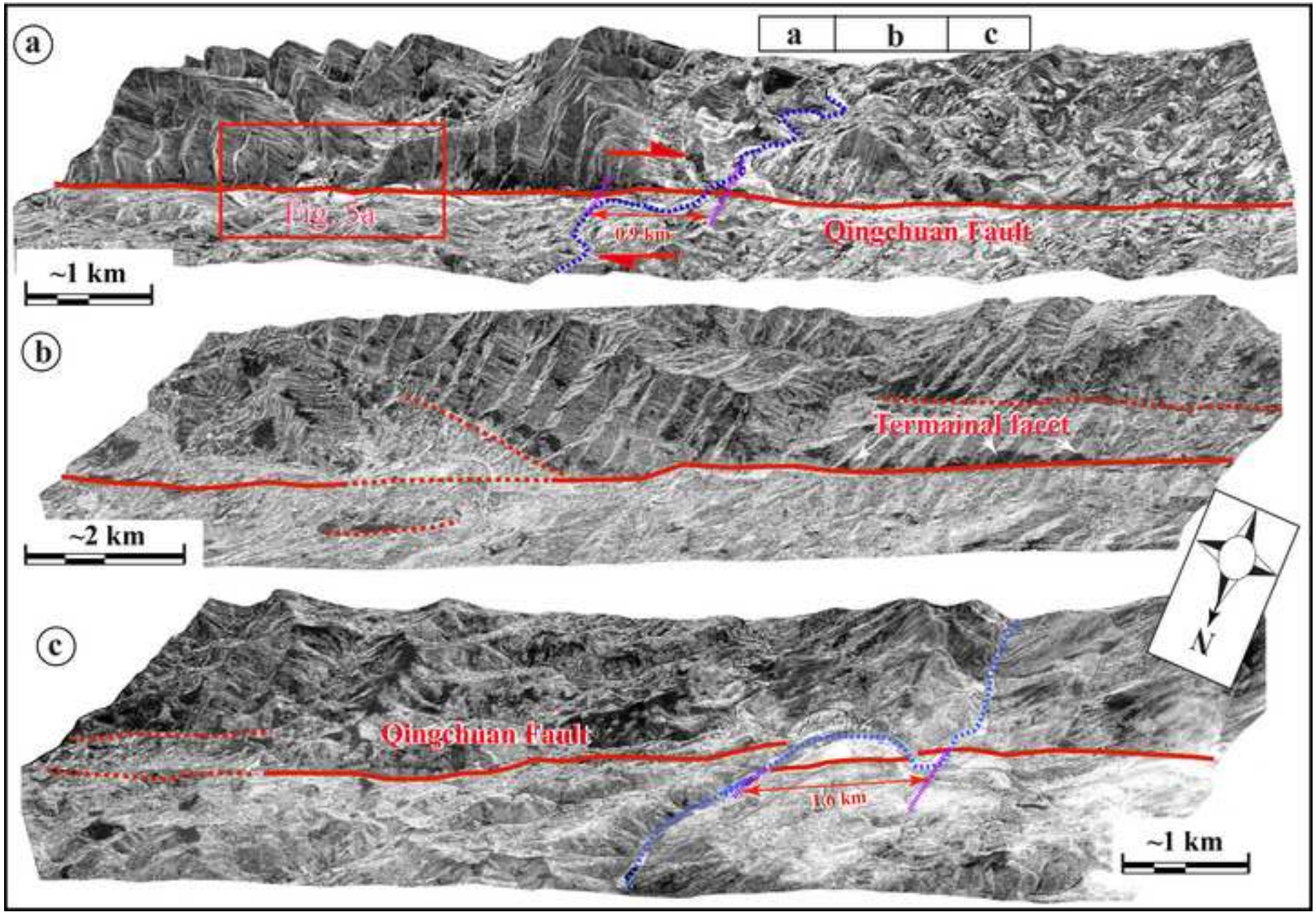

Figure5

Click here to download high resolution image

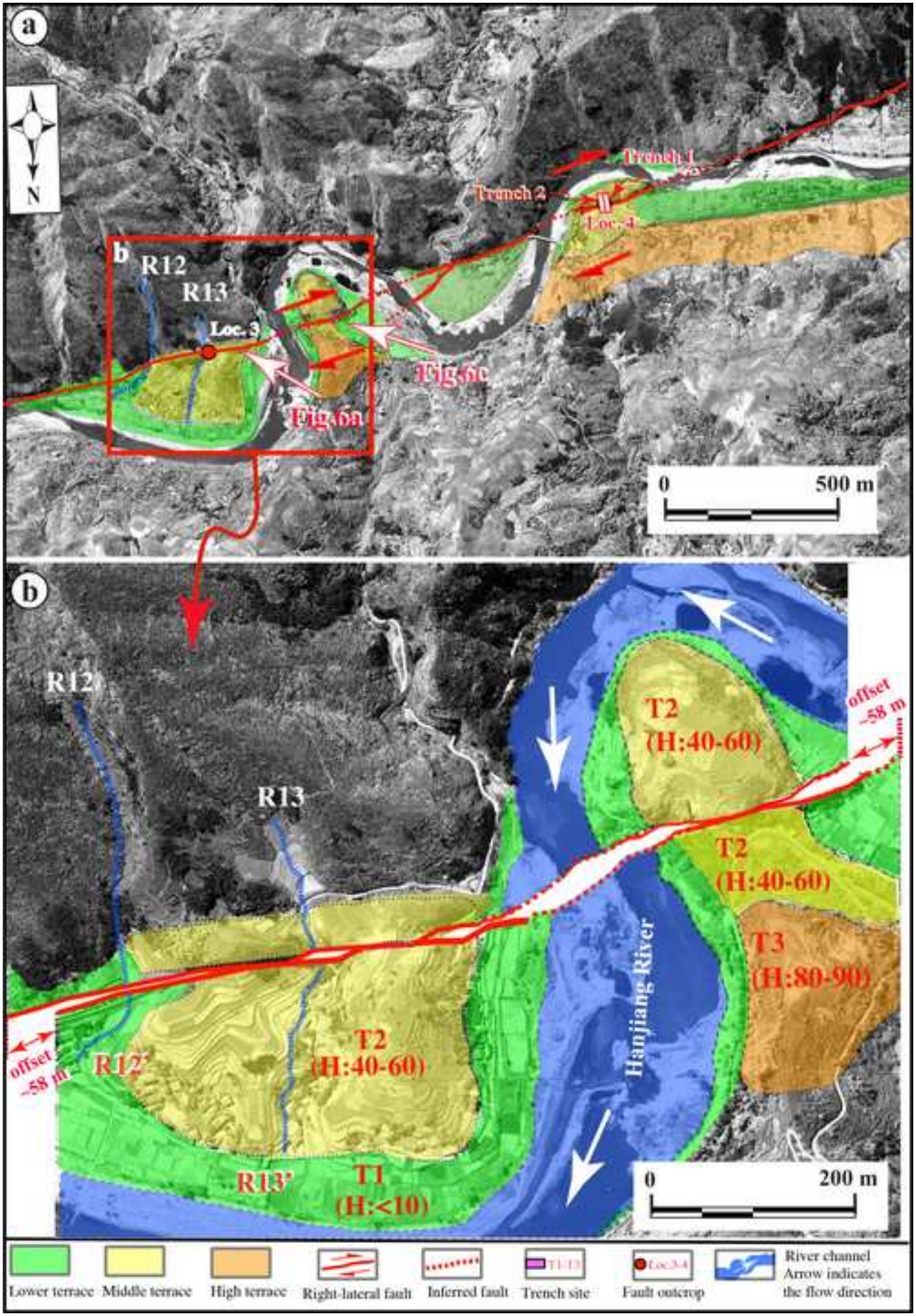

Figure6

Click here to download high resolution image

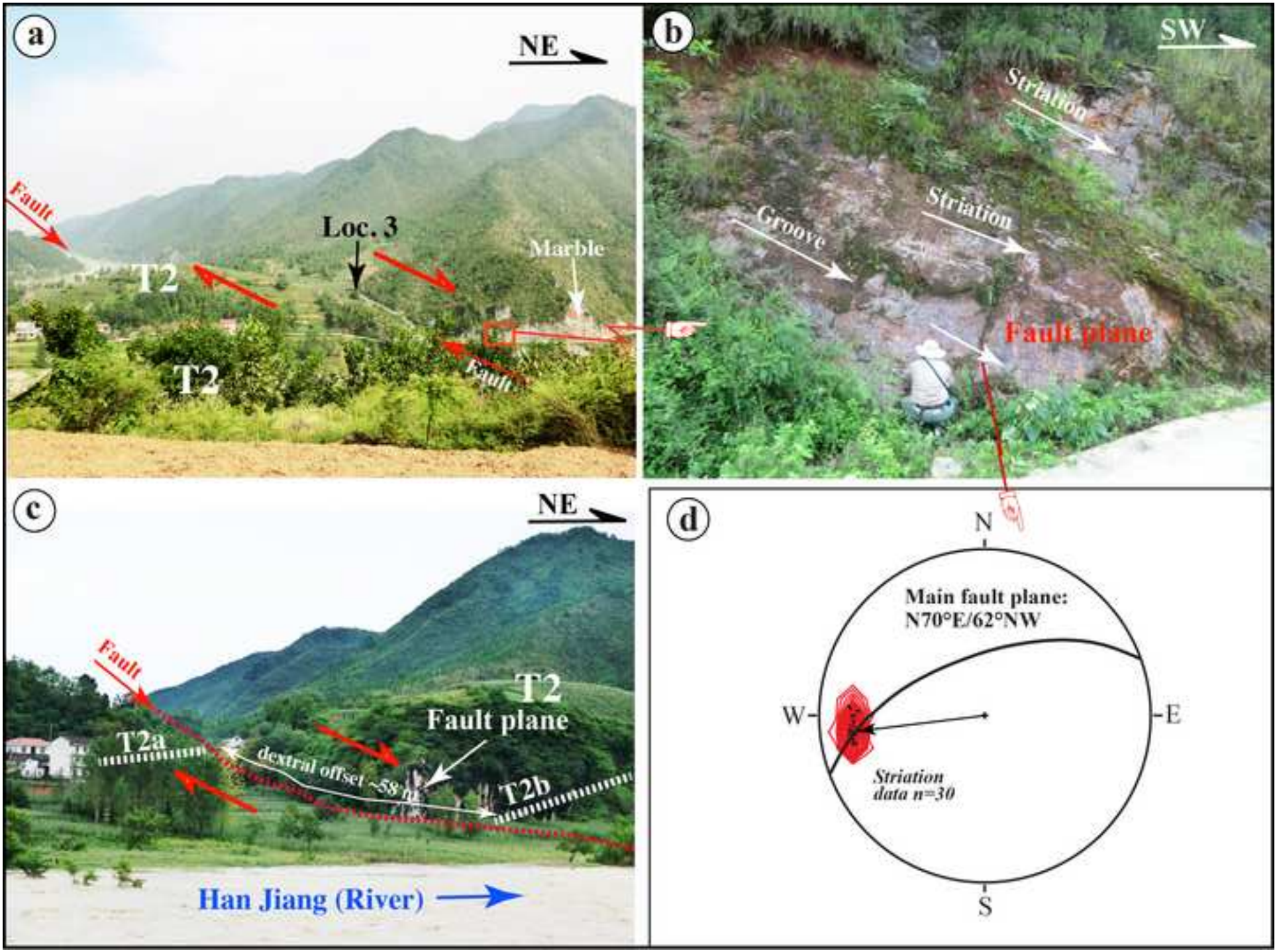

Figure7

Click here to download high resolution image

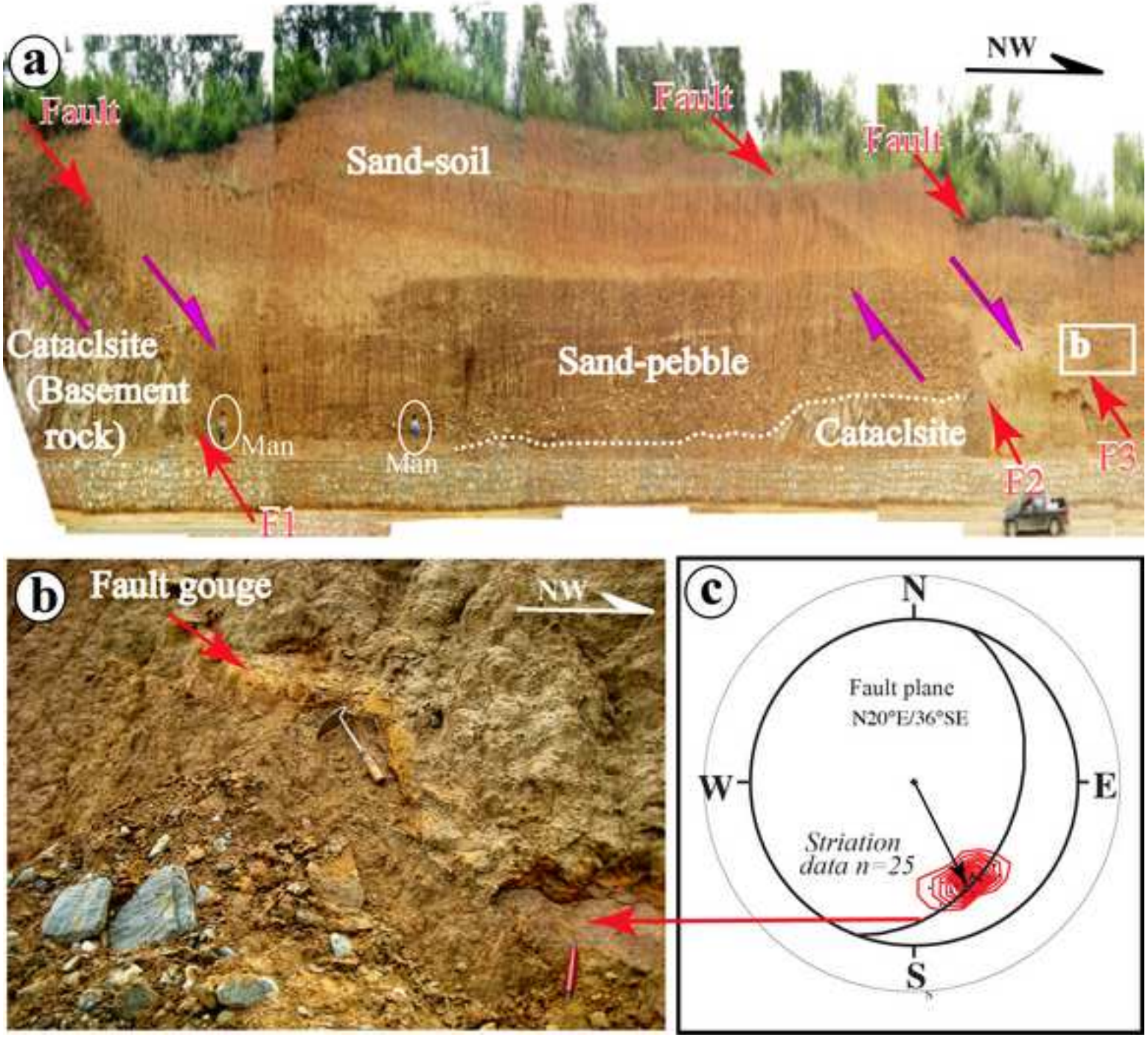

Figure8

Click here to download high resolution image

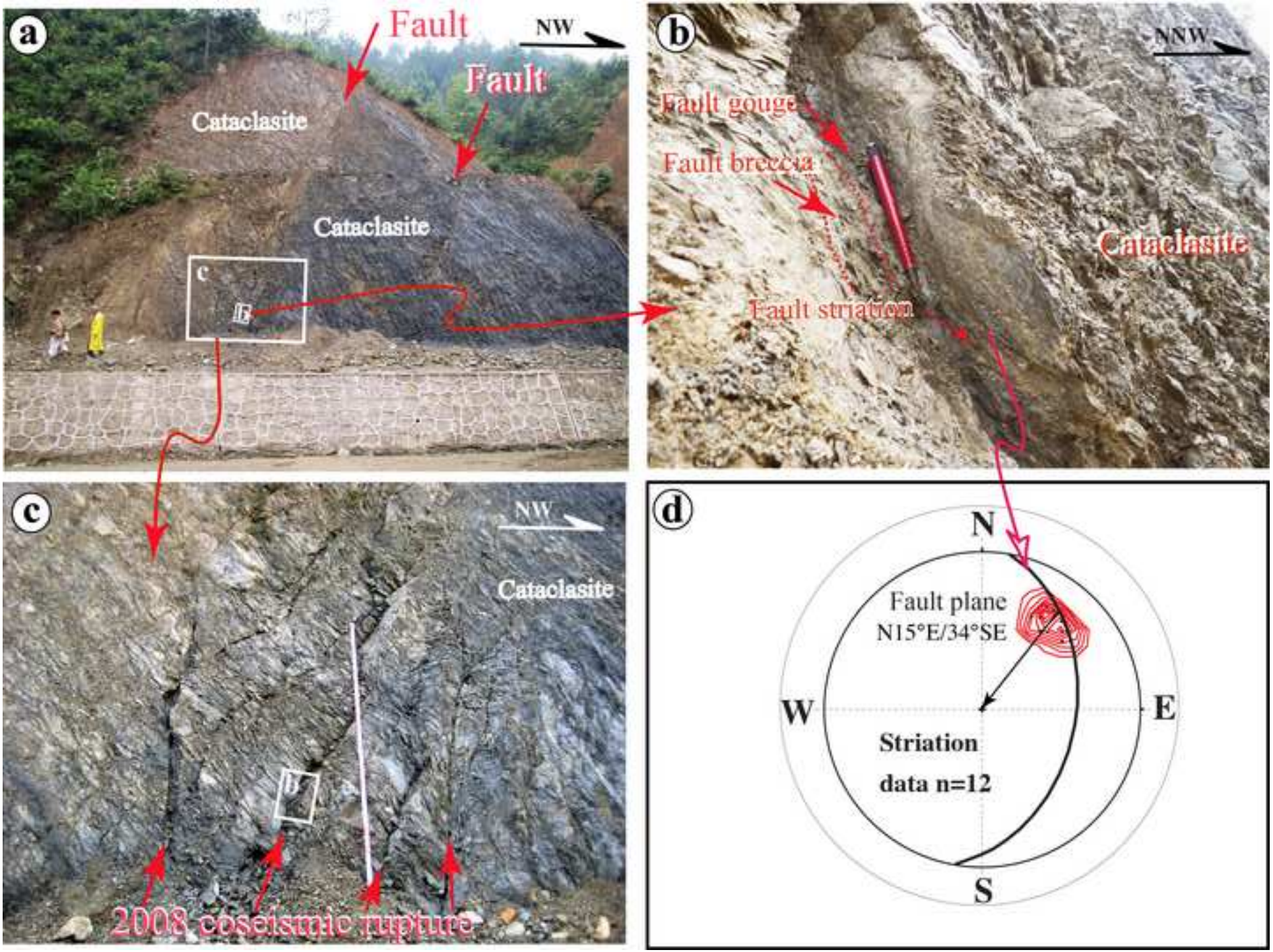

Figure9

Click here to download high resolution image

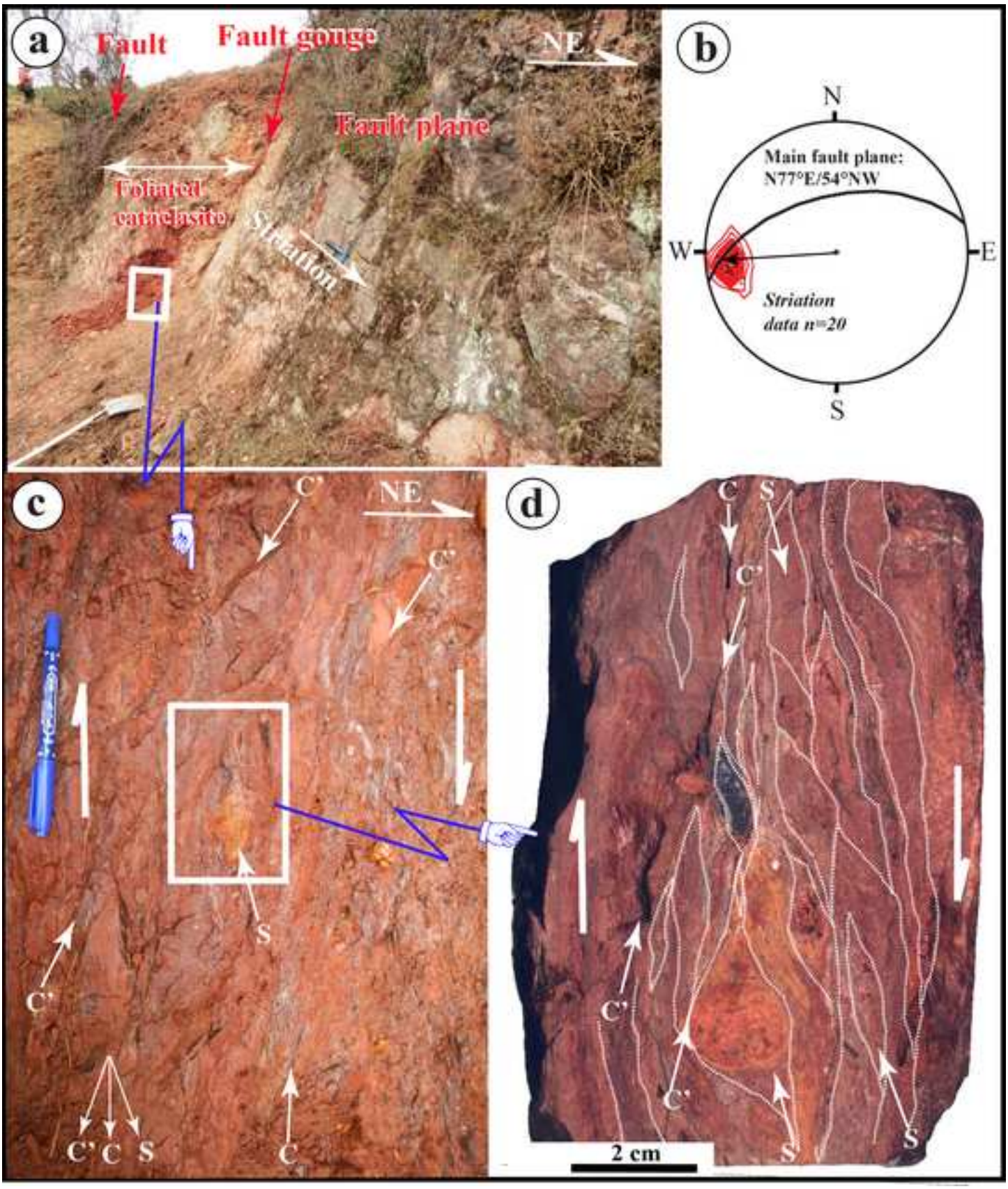

Figure10

Click here to download high resolution image

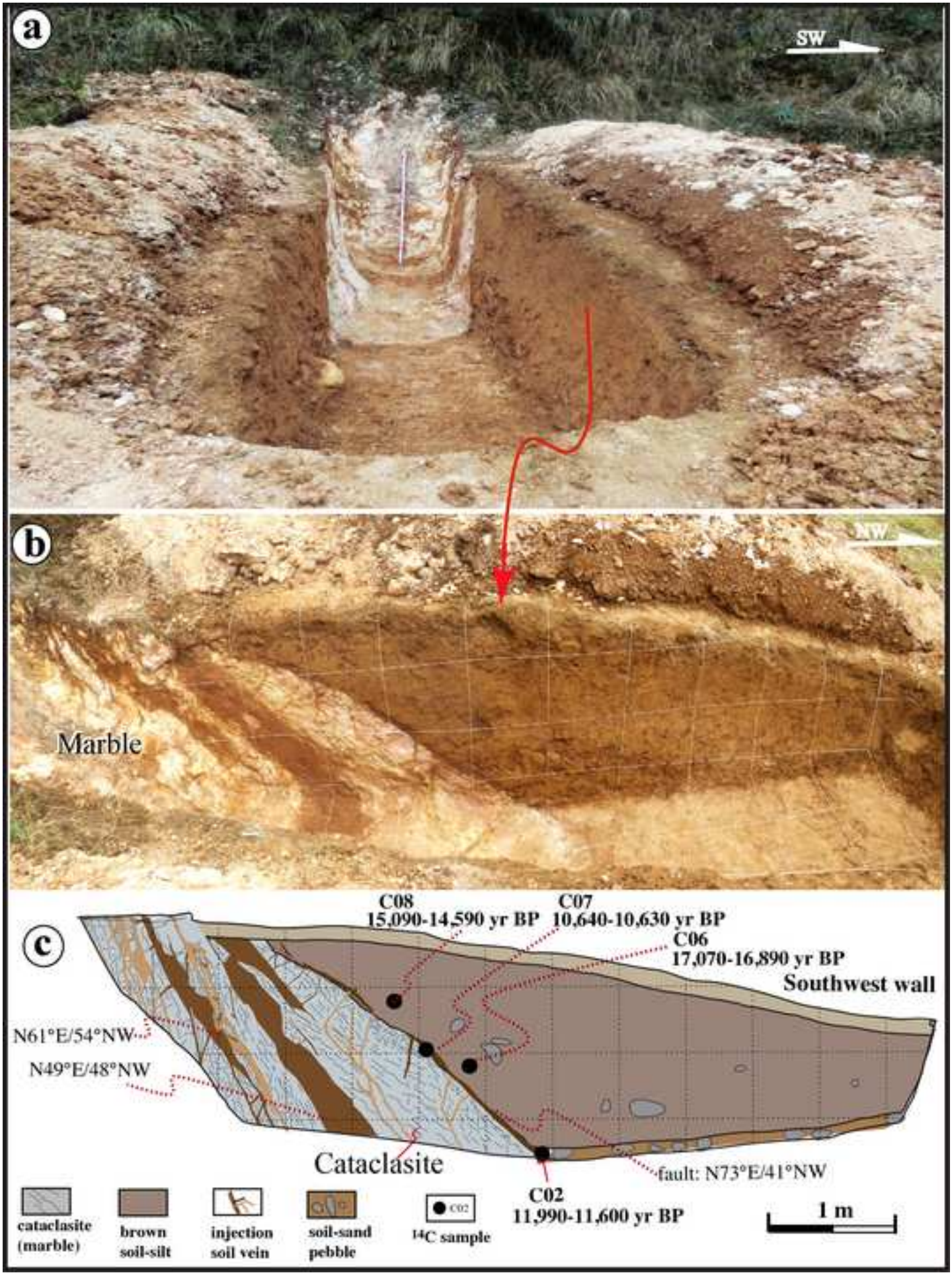

Figure11

Click here to download high resolution image

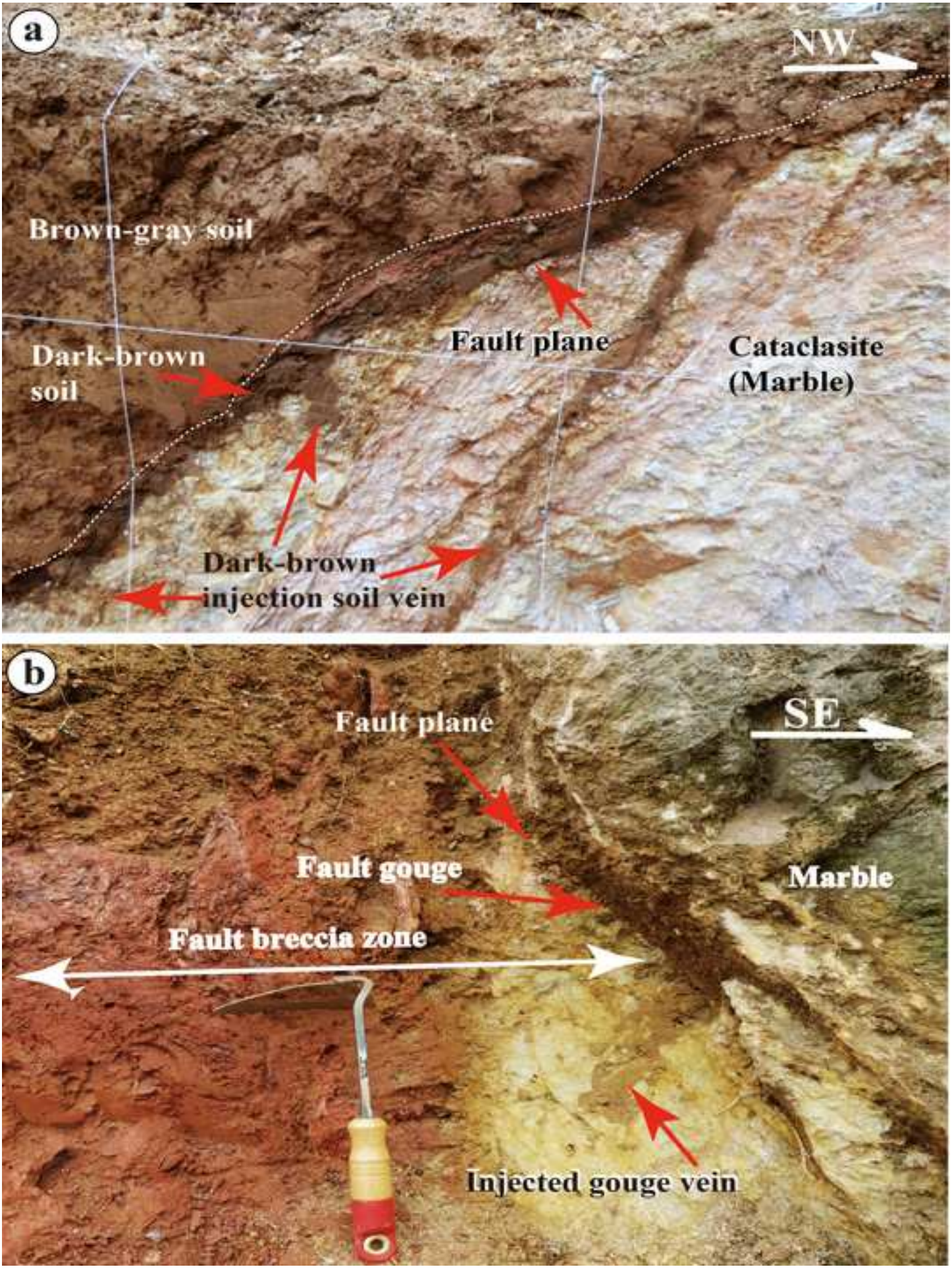

Figure12
Click here to download high resolution image

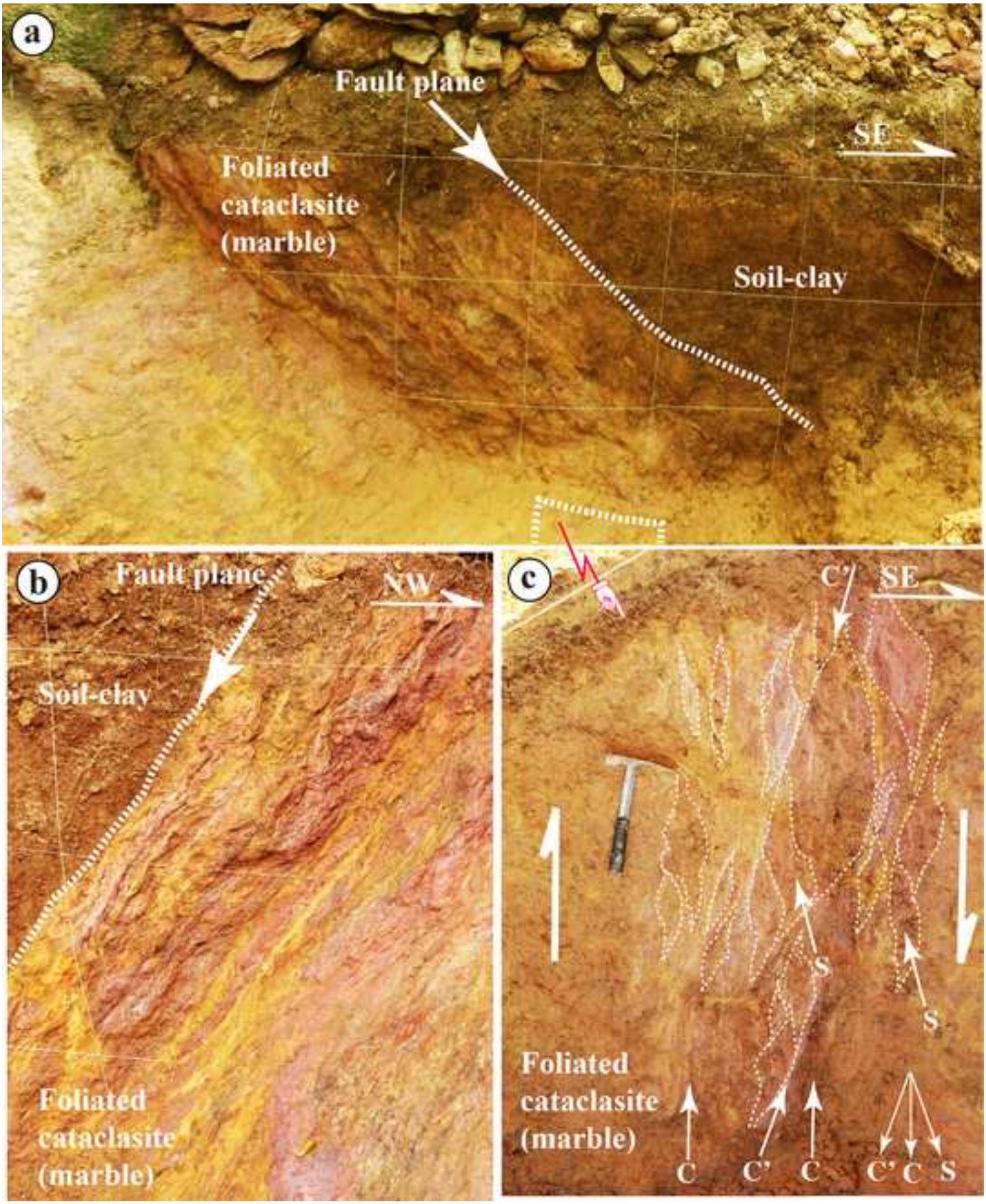

Figure13

Click here to download high resolution image

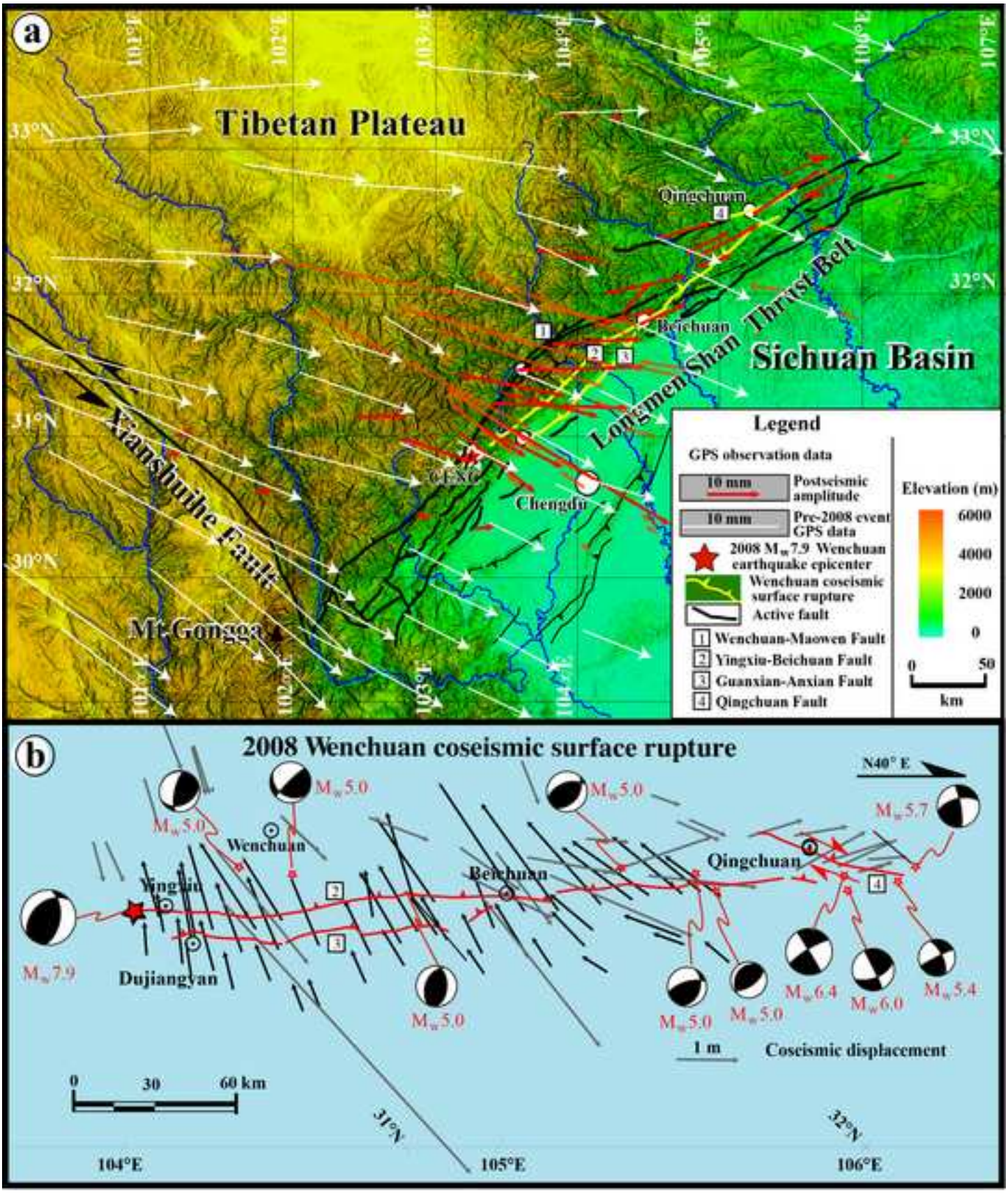

Table1

Table 1. Results of ^{14}C dating.				
Sample no[a].	Lab no.	Material	^{14}C age (yr BP) [b]	Calendar year range (2σ) [c]
C02	Beta-320142	organic soil	10,980 ± 50	11,990–11,600 yr BP
C06	Beta-320146	organic soil	13,940 ± 60	17,070–16,890 yr BP
C07	Beta-320147	organic soil	9,290 ± 50	10,640–10,630 yr BP
C08	Beta-320148	organic soil	12,590 ± 60	15,090–14,590 yr BP

[a]Samples were analyzed at Beta Analytic Inc. USA, via accelerator mass spectrometry (AMS).

[b]Radiocarbon ages were measured using accelerator mass spectrometry referenced to the year A.D. 1950. Analytical uncertainties are reported at 2σ.

[c]Dendrochronologically calibrated calendar age by Method A from CALIB Radiocarbon Calibration Version 6.1 (Stuiver et al., 2003).

Color-marked text

Click here to download Supporting Material: 4.Lin_JSG-2014-text-R2-color.doc